Title:

The role of geometrical features of the microarchitecture in the cancellous stiffness of the bovine femoral bone

Authors:

Satoshi Yamada[a,*], Koichi Fukasawa[b], Yuki Suzuki[b], Yuta Takahashi[b], Masahiro Todoh[a], Shigeru Tadano[c]

Affiliations:

[a] Division of Mechanical and Aerospace Engineering, Faculty of Engineering, Hokkaido University, N13 W8, Kita-ku, Sapporo, Hokkaido 0608628, Japan

[b] Division of Human Mechanical Systems and Design, Graduate School of Engineering, Hokkaido University, N13 W8, Kita-ku, Sapporo, Hokkaido 0608628, Japan

[c] Emeritus Professor, Hokkaido University, N13 W8, Kita-ku, Sapporo, Hokkaido 0608628, Japan

***Corresponding author:**

Satoshi Yamada, Ph.D.

Assistant Professor in Division of Mechanical and Aerospace Engineering, Faculty of Engineering, Hokkaido University

Postal address: N13 W8, Kita-ku, Sapporo, Hokkaido 0608628, Japan

Tel/Fax: +81-11-706-6406

E-mail: syamada@eng.hokudai.ac.jp

Keywords:

Biomechanics, Cancellous bone, Stiffness, Microarchitecture, Trabecular network, Single trabecula

Types of article:

Full paper

Abstract

This study aims to describe the geometrical features of single trabeculae and their network to explain cancellous stiffness as a representative mechanical function from a strength of materials perspective. Compression tests were performed on cancellous bone specimens dissected from a bovine femur as 5-mm cubes to measure cancellous stiffness. The microarchitecture was determined by microfocus X-ray computed tomography, and conventional morphological indicators were analyzed. The length, orientation, and bifurcation characteristics of each trabecula were analyzed by skeletonizing and linearizing the cancellous bone volume. Multiple regression analyses revealed a significant contribution made to cancellous stiffness by the compressive shape factor of the stiffness of single trabeculae, the trabecular orientation, and the bifurcation count, which evaluated the mean number of connected trabeculae at bifurcation points. Bifurcation count made the most significant contribution to cancellous stiffness. The combination of these geometrical indicators expressed the cancellous stiffness (R^2 = 0.85), which indicated as high accuracy as that explained by bone volume fraction, in specific bones that were not affected by bone disease or aging.

The present study demonstrated mechanically important geometrical features of the microarchitecture and indicated their complex contributions to cancellous stiffness underlying the contribution of bone volume fraction.

1. Introduction

Osteoporotic fractures often occur in areas such as the proximal femur, vertebrae, and distal forearm, which predominantly consist of cancellous bone. To understand the decline in the mechanical function of bone, which may underlie osteoporotic fractures, clarifying the determination mechanism of the mechanical properties of cancellous bone is essential. As Ulrich et al. and Greenwood et al. have pointed out, the mechanical properties of cancellous bone have been evaluated using three-dimensional microarchitecture and its combinations [1,2]. Conventional morphological indicators of cancellous bone microarchitecture have been proposed and widely used [3], and it is well known that bone volume fraction is highly correlated with cancellous bone stiffness [4]. In general, from a strength of materials perspective, cancellous stiffness, i.e., the macroscopic apparent elastic modulus as an indicator of mechanical function, is theoretically determined by the stiffness of single trabeculae, depending on trabecular shape and material properties; trabecular orientation; and the three-dimensional connections between single trabeculae. However, these components have not been sufficiently evaluated directly using the conventional indicators. Various combinations of the structural features are possible, even at the same volume fraction. Therefore, further investigation of the mechanically important structural features and their combined contributions underlying the correlation of the bone volume fraction are needed to elucidate the determination mechanism of the mechanical functions of cancellous bone and to understand the significant control targets for the increase of the mechanical functions.

In addition to conventional indicators, some features of trabecular morphology and network structure have been reported. Local bone morphometry methods by decomposition of single trabeculae into rods and plates have been proposed [5,6], and a few studies have evaluated trabecular length [7-10]. The relationships of local bone morphometry to cancellous stiffness and ultimate stress have been noted [7,8,10]. However, to clarify the contributions of single trabeculae to cancellous stiffness, shape factors composed of its length and cross-sectional dimensions that determine the stiffness of a single trabecula may be essential, even though their components have been partially evaluated. Furthermore, Reznikov et al. skeletonized cancellous bone and investigated intertrabecular angles at bifurcation points [11].

However, the mechanical contributions of the bifurcation characteristics to cancellous stiffness have not been elucidated. To understand the determination mechanism of the mechanical properties of cancellous bone, the combinations of such geometrical features need to be investigated. Therefore, this study evaluated the geometrical features of single trabeculae and their network based on the skeletonized network to demonstrate mechanically important features of the microarchitecture.

The influence of the mechanical properties of a single trabecula to the analysis of the contributions of the microarchitecture also needs to be considered. Some studies have performed micromechanical tests on single trabeculae with technical challenges [12,13]. Tensile [14-22] and three-point bending tests [15,16,23-26] have been performed. The authors have also previously demonstrated a microcantilever-bending test of the measurements of the elastic properties of a single trabecula [27]. However, no studies have experimentally elucidated the site-specific differences in the mechanical properties of a single trabecula by the micromechanical tests and their contributions to the distribution of cancellous stiffness. The present study confirmed the lower impact of the differences in the elastic modulus of a single trabecula on the distribution of cancellous stiffness in the analysis of the contributions of the geometrical features.

Therefore, the present study hypothesizes that cancellous stiffness is determined by the combination of the stiffness, orientation, and bifurcation characteristics of single trabeculae and aims to describe geometrical features of the microarchitecture from a strength of materials perspective to explain cancellous stiffness and to clarify the dominant elements.

2. Materials and Methods

2.1 Specimen preparation

The present study used 22–25 month old female bovines raised as livestock and obtained from local agricultural cooperatives. Cubic cancellous bone specimens were dissected from the right femur of a bovine (Bovine A), which was stored at −30°C. Twelve and eleven specimens were isolated from the metaphysis and neck regions defined as shown in Fig. 1a, respectively. The specimens were collected in $5 \times 5 \times 5\ \mathrm{mm}^3$ cubes using a low-speed diamond wheel saw (Model 650, South Bay

Technology, USA) while sprinkling water on the collection site. The bone marrow was not removed. The three axes of the cubic specimens were aligned to the lateromedial, anteroposterior, and proximodistal directions of the femur (Fig. 1b). The microarchitecture of the specimens was determined using a microfocus X-ray computed tomography (CT) scanner (inspeXio SMX-90CT, Shimadzu Corporation, Japan) at a voxel size of 0.015 mm/voxel. Each specimen was stored at −30°C and completely thawed to 4°C before mechanical tests.

2.2 Compression tests

Uniaxial compression tests of the specimens were performed in the femoral axis in ambient air at room temperature using a material testing machine (Model 3365, Instron, USA). Cancellous stiffness (E_c) was obtained as the apparent elastic modulus of the specimens. The specimens were loaded to a displacement of 0.1 mm at a speed of 0.1 mm/min after a preloading of 20 N and a preconditioning cycle of loading and unloading performed at the same displacement and speed as those of the intended test. The E_c was calculated from the load–displacement relationship between 50% and 80%

of the maximum load in the intended test.

2.3 Microarchitecture analysis

The specimen regions in the micro-CT images were extracted using ImageJ software (National Institutes of Health, USA), and the bone volume was obtained by binarizing the images using the optimal thresholding method [28,29] of the BoneJ plug-in [30] (Fig. 2a). Among the conventional morphological indicators of the microarchitecture reviewed by Bouxsein et al. [3], the following were analyzed using BoneJ functions: bone volume fraction (*BV/TV*), connectivity density (*Conn.D*), structure model index (*SMI*), degree of anisotropy (*DA*), trabecular thickness (*Tb.Th*), and trabecular separation (*Tb.Sp*).

Geometrical indicators of the microarchitecture, such as the number, length, and orientation of single trabeculae, the number of bifurcation points, and bifurcation characteristics in the specimens, were evaluated by skeletonizing (Fig. 2b) and linearizing the bone volume (Fig. 2c). By skeletonizing the thresholded images on BoneJ [31,32], branches and junctions of skeletonized cancellous bone were obtained.

However, many short branches were included due to the nonuniform shape of the bone volume, and their lengths did not represent the trabecular length of the network. Therefore, these artifacts were removed using a customized program on MATLAB (MathWorks, USA). First, dots and branches without connections to any branches were removed. Second, short needle-like branches were removed, and bent branches were replaced with a straight skeleton (Fig. 3a). Both ends of the straight skeletons were defined as bifurcation points. In the case of overlapping straight skeletons, one was retained and the others were removed (Fig. 3b). Straight skeletons without connections to other branches were also removed. Still, many short branches that connected to the junctions connecting three or more branches remained (Fig. 3c). Therefore, these short branches were removed, and the branches connected at both ends of the removed short branches were reconnected at the midpoint of the removed branches, which resulted in a new bifurcation point. This was performed sequentially starting from the shortest branch. However, the short branches that were part of a generated triangle were preserved to maintain the network structure (Fig. 3d). If the short branches of triangles were removed, the triangle turns to overlapping straight skeletons, and the network structure partially disappears. However, if the short branches of other polygons are processed, the impact on the network structure is negligible. The threshold of the branch length was set to 150 μm.

The number of straight skeletons with a length of 150 μm or more per 1 mm^3 in each specimen was calculated as n_t, and the mean length was calculated as $\bar{l}$. The compressive and cantilever-bending stiffness of a circular cylinder are represented as $\frac{\pi t^2}{4l}E$ and $\frac{3\pi t^4}{64l^3}E$ respectively, with a diameter of t, a length of l, and an elastic modulus of E. To evaluate the compressive and bending shape factors of the stiffness of single trabeculae within each specimen, $Tb.Th^2/\bar{l}$ and $Tb.Th^4/\bar{l}^3$ were designated as *CSF* and *BSF*, respectively. Furthermore, the orientation angle θ of each straight skeleton with respect to the femoral axis was analyzed, and the mean angle was calculated as $\bar{\theta}$.

The number of bifurcation points per 1 mm^3 was calculated as n_b, including the number of edges of straight skeletons. The number of connecting straight skeletons at a bifurcation point was defined as the bifurcation count b, and the mean bifurcation count of each specimen was calculated as $\bar{b}$. The angle between two straight skeletons at a bifurcation point was defined as the bifurcation angle ϕ, and the mean angle $\bar{\phi}$ of each specimen was calculated. The mean angles at the bifurcation counts in each specimen were also calculated.

The results of the processing steps of the customized program were verified via the manual analysis of five regions of the trabecular network containing 50 connected branches extracted from the specimens.

2.4 Elastic modulus measurements of a single trabecula

Single trabecula specimens were also dissected from the right femur of another bovine (Bovine B), which was stored at −30°C and did not differ significantly in length with that of Bovine A. Ten single trabeculae were selected in the metaphysis, which have been previously measured [27], and nine single trabeculae were selected in the neck region. A rod-like single trabecula was isolated while ensuring that one extremity remained connected to the other trabeculae, using the wheel saw while sprinkling water on the sampling site (Fig. 1c). The orientation angle θ of the isolated trabecula was visualized by micro-CT scanning at 0.092 mm/voxel. The remaining attached cancellous bone portion was shaped into a small rectangle (Fig. 1d). After air-drying, the specimen was placed vertically into a holder and fixed using epoxy resin (Fig. 1e). The shape of the single trabecula was obtained by scanning at 0.009 mm/voxel. The specimens were stored in sealed cases at room temperature.

Elastic moduli of the single trabecula specimens were measured by microcantilever-bending tests in the air at room temperature using a customized testing device (Fig. 4). The position adjacent to the free end of the specimen was horizontally subjected to the load F by displacing a loading plate using a uniaxial stage. Specimen images were captured by microscopy in a vertical position to measure the deflection d of the contact position. The cantilever length L was the distance between the contact position and the fixed end. The specimens were approximated to a circular cylinder and the diameter D was calculated from the average cross-sectional area. The tissue was assumed to be an orthotropic material with a principal axis that corresponded to the longitudinal axis. Based on the Euler–Bernoulli beam theory, the deflection of the contact position is described in Eq. (1) [33]:

$$d = \frac{64L^3}{3\pi D^4 E_t} F \qquad (1),$$

where E_t is the elastic modulus in the longitudinal axis. The E_t was calculated from the mean gradient F/d of three force–deflection relationships. Two specimens in the neck region with $L \leq 2.22\ D$ were excluded from the results.

2.5 Statistical analyses

Simple correlation analyses were performed with respect to E_c for the microarchitecture indicators, and Pearson's correlation coefficients r were analyzed. The correlations of trabecular orientation were evaluated using the cosine of the mean angle, $\cos\bar{\theta}$. Furthermore, multiple linear regression analyses were performed with respect to E_c for the combinations of the indicators that were statistically correlated with E_c, excluding the indicators that were mutually correlated because of multicollinearity. Adjusted coefficients of determination R^2 were analyzed for the combinations with statistically significant standardized partial regression coefficients β. The significance level was set to 0.05.

2.6 Verification of the effect of the experimental moist conditions

The cancellous bone specimens were not air dried; however, they were exposed to air during short-term CT imaging and mechanical testing in this study. For verification, 14 cubic specimens were further extracted from the proximal femur of another bovine (Bovine C). Two compression tests using the same protocol were performed in air using seven specimens, and E_c was compared between the two tests. Using the remaining seven specimens, a compression test was performed in air, followed by another test that was performed in saline at room temperature after immersion in saline solution for 24 h. E_c was also compared between the two conditions.

The effect of the moist conditions of single trabecula specimens on the order of magnitude of the elastic modulus was also verified. An additional six single trabeculae were extracted from the proximal femurs of two bovines (Bovines C and D), and E_t was measured under air-drying conditions. Then, the specimens were immersed in saline solution for 24 h and were examined again inside a small water bath containing saline solution at room temperature.

3. Results

The E_c were 332.9 ± 88.3 MPa in the metaphysis and 523.7 ± 55.9 MPa in the neck region, respectively, and differed significantly (Table 1). Among the morphological indicators, *BV/TV*, *Conn.D*, *SMI*, and *Tb.Sp* differed significantly between the two regions. All geometrical indicators also varied significantly, except $\bar{\theta}$. As shown in Table 2, the mean bifurcation angle at each bifurcation count did not differ significantly between the two regions.

Table 1. Means and standard deviations of cancellous stiffness E_c and morphological and geometrical indicators of the cancellous bone specimens

			Metaphysis (n = 12)		Neck (n = 11)		Statistical	r-value
		Unit	Mean	S.D.	Mean	S.D.	difference	with E_c
Cancellous stiffness	E_c	MPa	332.9	88.3	523.7	55.9	$P < 0.01$	-
Morphological indicators	*BV/TV*		0.195	0.026	0.299	0.036	$P < 0.01$	0.93 **
	Conn.D	/mm^3	3.52	0.46	6.85	3.25	$P < 0.01$	0.36
	SMI		1.67	0.24	1.05	0.26	$P < 0.01$	−0.95 **
	DA		0.68	0.09	0.66	0.11	*n.s.*	0.33
	Tb.Th	mm	0.203	0.008	0.214	0.034	*n.s.*	0.47 *
	Tb.Sp	mm	0.851	0.077	0.611	0.053	$P < 0.01$	−0.89 **
Geometrical indicators	n_t	/mm^3	8.30	0.93	15.62	5.98	$P < 0.01$	0.45 *
	$\bar{l}$	mm	0.481	0.012	0.425	0.048	$P < 0.01$	−0.35
	CSF	mm	0.086	0.007	0.109	0.025	$P < 0.05$	0.68 **
	BSF	mm	0.016	0.003	0.028	0.011	$P < 0.01$	0.72 **
	$\bar{\theta}$	degree	53.5	1.2	53.2	1.6	*n.s.*	
	$\cos\bar{\theta}$		0.595	0.017	0.598	0.022	*n.s.*	0.50 *
	n_b	/mm^3	5.29	0.55	9.43	3.16	$P < 0.01$	0.48 *
	$\bar{b}$		3.34	0.03	3.47	0.09	$P < 0.01$	0.53 **
	$\bar{\phi}$	degree	109.8	0.5	108.1	0.7	$P < 0.01$	−0.80 **

BV/TV, bone volume fraction; *Conn.D*, connectivity density; *SMI*, structure model index; *DA*, degree of anisotropy; *Tb.Th*, trabecular thickness; *Tb.Sp*, trabecular separation; n_t, number of straight skeletons per 1 mm^3 in each specimen; $\bar{l}$, mean trabecular length; *CSF*, compressive shape factor of the stiffness of single trabeculae; *BSF*, bending shape factor of the stiffness of single trabeculae; $\bar{\theta}$, mean orientation angle; n_b, number of bifurcation points per 1 mm^3; $\bar{b}$, mean of bifurcation count; $\bar{\phi}$, mean bifurcation angle; *n.s.*, no significant difference. The r-values indicate Pearson's correlation coefficients between E_c and the indicators. *$P < 0.05$; **$P < 0.01$.

Table 2. Means and standard deviations of bifurcation angles at triple, quadruple, quintuple, and sextuple bifurcation points

		ϕ, degree						
		Metaphysis		Neck		All		Statistical difference
		Mean	S.D.	Mean	S.D.	Mean	S.D.	in two regions
b	3	113.9	0.4	113.7	0.5	113.8	0.5	*n.s.*
	4	106.4	0.8	105.8	0.9	106.1	0.9	*n.s.*
	5	102.3	1.7	101.9	0.6	102.1	1.3	*n.s.*
	6	98.4	3.9	99.2	1.6	98.8	3.0	*n.s.*

b, bifurcation count; ϕ, bifurcation angle; *n.s.*, no significant difference.

The *BV/TV*, *Tb.Th*, n_t, *CSF*, *BSF*, $\cos\bar{\theta}$, n_b, and $\bar{b}$ were positively correlated with E_c, whereas *SMI*, *Tb.Sp*, and $\bar{\phi}$ were negatively correlated (Table 1 and Fig. 5). All morphological indicators except *DA* showed statistical correlations with *BV/TV*. Furthermore, significant correlations were found within the combinations of n_t, $\bar{l}$, n_b, $\bar{b}$, and $\bar{\phi}$; $\bar{l}$ and $\cos\bar{\theta}$; and *CSF*, *BSF*, and $\bar{\phi}$. Multiple regression analyses showed significant β-values with high R^2 values in the combinations of geometrical indicators (Table 3): *CSF*, $\cos\bar{\theta}$, and $\bar{b}$ ($R^2 = 0.85$); *CSF*, $\cos\bar{\theta}$, and n_b ($R^2 = 0.85$); *BSF*, $\cos\bar{\theta}$, and $\bar{b}$ ($R^2 = 0.84$); *BSF*, $\cos\bar{\theta}$, and n_b ($R^2 = 0.84$); n_t, *CSF*, and $\cos\bar{\theta}$ ($R^2 = 0.84$); n_t, *BSF*, and $\cos\bar{\theta}$ ($R^2 = 0.83$); and $\cos\bar{\theta}$ and $\bar{\phi}$ ($R^2 = 0.83$). The R^2 between E_c and *BV/TV* was 0.86. The multiple regression equation of *CSF*, $\cos\bar{\theta}$, and $\bar{b}$ is expressed by Eq. (2):

$$E_c = 0.365\, CSF + 0.560 \cos\bar{\theta} + 0.641\, \bar{b} \quad (2),$$

where all variables were standardized, and r-value of $\bar{b}$ was the highest among $\bar{b}$, n_t, and n_b. The coefficient of each variable in the equation was β. The β-values of the bifurcation indicators were the largest in each combination of geometrical indicators (Table 3). As shown in Fig. 6, no significant difference was found in the two correlations between the standardized measured values of E_c and standardized estimated values obtained using the regression equation of *BV/TV* or Eq. (2).

Table 3. Standardized partial regression coefficients β of each indicator and adjusted coefficients of determination R^2 in multiple linear regression analyses

Combinations of geometrical indicators			β			R^2
CSF	$\cos\bar{\theta}$	$\bar{b}$	0.365	0.560	0.641	0.85
CSF	$\cos\bar{\theta}$	n_b	0.455	0.524	0.620	0.85
BSF	$\cos\bar{\theta}$	$\bar{b}$	0.366	0.578	0.588	0.84
BSF	$\cos\bar{\theta}$	n_b	0.447	0.549	0.555	0.84
n_t	*CSF*	$\cos\bar{\theta}$	0.614	0.471	0.531	0.84
n_t	*BSF*	$\cos\bar{\theta}$	0.546	0.464	0.554	0.83
$\cos\bar{\theta}$	$\bar{\phi}$		0.459	−0.776		0.83

The E_t were 9.1 ± 5.4 GPa in the metaphysis [27] and 11.5 ± 4.6 GPa in the neck region, respectively, and did not differ significantly (Table 4). The examined specimen orientation and size are shown in Table 4.

Table 4. Means and standard deviations of orientation, size, and elastic modulus of the single trabecula specimens in the metaphysis, neck, and all regions.

			Metaphysis (n = 10) [27]		Neck (n = 7)		All (n = 17)	
		Unit	Mean	S.D.	Mean	S.D.	Mean	S.D.
Specimen orientation and size	θ	degree	49	24	38	23	45	24
	D	mm	0.254	0.099	0.147	0.024	0.210	0.093
	L	mm	1.12	0.17	0.39	0.05	0.82	0.39
Elastic modulus	E_t	GPa	9.1	5.4	11.5	4.6	10.1	5.1
	R^2		0.96	0.02	0.99	0.00	0.98	0.02

θ, orientation angle; D, approximate diameter; L, cantilever length; E_t, elastic modulus; R^2, coefficient of determination in force–deflection relationships.

In the verification performed using cancellous bone specimens, no significant difference was detected in the E_c between the two tests performed in air. Furthermore, no significant difference was detected between the two experimental environments. In the verification performed using single trabecula specimens, the E_t values were 8.7 ± 2.2 and 5.2 ± 2.2 GPa under the air-dried and rehydrated conditions, respectively, and varied significantly ($P < 0.01$). However, a positive correlation between the conditions was observed ($r = 0.84$, $P < 0.05$).

4. Discussion

This study hypothesized that cancellous stiffness is determined by the combination of the stiffness, orientation, and bifurcation characteristics of single trabeculae. The present findings revealed the contribution made to cancellous stiffness by the compressive shape factor of the stiffness of single trabeculae, the trabecular orientation, and the bifurcation count. Notably, bifurcation count made the most significant contribution to cancellous stiffness in the multiple regression analysis. Furthermore, the combination of these geometrical indicators expressed the cancellous stiffness with an accuracy that was as high as that of the bone volume fraction.

In the compression tests of the cancellous bone specimens, the stress-strain curves did not show a macroscopic yield point and the calculation regions of cancellous stiffness exhibited high linearity ($R^2 > 0.99$). The maximum deformation applied in the present study was also set within the elastic region, according to a previous study [4]. Furthermore, the absence of significant difference in cancellous stiffness between the two tests performed in air suggests a steady compression testing. Brear et al. pointed out that the temperature in a moist environment did not significantly affect the cancellous stiffness [34]. Therefore, the findings of an absence of significant differences between the two tests performed in air and between the two experimental moist conditions, respectively, suggest that the experimental procedures in the present study had little impact on the results.

The average E_t was 10.1 ± 5.1 GPa, which was within the range of 4.4–17.1 GPa range reported in previous micromechanical tests of dry bovine trabeculae involving different measurement methods and collection sites [15,17,22]. In the microcantilever-bending tests, the effect of shear forces on the deflection was neglected in the calculations; however, it could be a source of error, especially in shorter trabecular lengths in comparison with the cross-section. In cantilever bending of a cylinder made of an isotropic material with an elastic modulus of E and a Poisson's ratio of v, the deflection d_s due to shear forces is expressed by Eq. (3) using the Cowper's shear coefficient in Timoshenko's beam theory [35]:

$$d_s = \frac{4(7+6v)FL}{3\pi D^2 E} \quad (3).$$

In the present study, the specimens in which the deflection of shear forces exceeded

10% of the total deflection assuming Eq. (3) and v of 0.3, i.e., $L \leq 2.22D$, were excluded from the results, and the included average effect was 4.8%.

Furthermore, the measurements of a single trabecula under wet conditions are not well-studied; this study also examined air-dried specimens. The trend of the elastic modulus of a single trabecula under the air-dried and rehydrated conditions corresponded to the trend in the literature [17]. However, the observed positive correlation between the conditions indicates a lesser impact on the order of magnitude. This finding suggests that air-drying has little impact on the comparison between the metaphyseal and neck regions. However, studies under a moist environment may be necessary to clarify the effects of aging or disease.

Multiple regression analyses showed that the combinations of shape factors, orientation, and bifurcation characteristics could explain the E_c. The n_t and n_b were correlated with $\bar{l}$, $\bar{b}$, and $\bar{\phi}$ and might be indirectly determined. This suggests that the microarchitecture represented by these features determines the E_c in the resulting volume fraction, which makes sense from the perspective of the strength of materials.

First, although the E_c at the neck region was significantly higher than that at the metaphysis, no significant difference in E_t was observed. This finding suggests that although variations in E_t exist, they do not directly contribute to the distribution of E_c within these regions. Conversely, *CSF* and *BSF* were positively correlated with E_c in the simple correlation analyses, which was higher than *Tb.Th* alone. Therefore, the indicators represent the shape effects that govern the stiffness of single trabeculae, which was hypothesized to partially determine E_c. However, the superiority of the shape factors to material properties may reflect the nature of the investigations, which were performed within a specific bone without bone disease or aging. Furthermore, the differences in correlation coefficients between *CSF* and *BSF* were minor, which may reflect to dispersion of the trabecular orientation in each specimen.

Second, the significant correlation detected between trabecular orientation and E_c and Eq. (2) demonstrated that trabecular orientation is a mechanically important feature of the microarchitecture. This factor has a potential to explain the anisotropy of the mechanical functions of cancellous bone, which cannot be explained using *BV/TV*. However, *DA* showed no correlation with E_c, which may reflect the differences between the testing direction and the strongest orientation. The dispersion of trabecular orientation may be useful in evaluating the mechanical anisotropy.

Third, the bifurcation angle corresponded to the bifurcation count with no significant difference between the two regions. The mean angle at each bifurcation count was close to the measurements reported by Reznikov et al. [11]. As they pointed out, this finding suggests that the single trabeculae tend to diverge isotropically according to the bifurcation count. Furthermore, $\bar{b}$ showed a positive correlation with E_c. Prot et al. found correlations between the numbers of triple and quadruple bifurcation points and mechanical properties [36]. These suggest that bifurcation count increases the stiffness around a bifurcation point, perhaps isotropically, and that the number of points with a large bifurcation count increases the E_c. Furthermore, β-values in the regression equation especially indicate the relatively significant influence of the bifurcation characteristics, which is also a new experimental finding. This leads to the conclusions that the effect of the stiffness of the bifurcation points on cancellous stiffness, which is indirectly evaluated by $\bar{b}$, is another important structural feature to consider in addition to the stiffness and orientation of single trabeculae.

Therefore, the combinations of these geometrical indicators express the cancellous stiffness, which supports our hypothesis and demonstrates the mechanically important structural features and their complex contributions underlying the correlation between the bone volume fraction and cancellous stiffness. However, the adjusted coefficients of determination are still comparable to that of the volume fraction, which might reflect the nature of the present investigation, which used specific bones that were not affected by bone disease or aging in the study.

The linearized process was performed after the skeletonization, which was partly similar to the method used by Reznikov et al. in removing short branches [11]. This is suitable in indicating the geometrical features of networks composed of rod- and plate-like trabeculae. However, in the present study, the shape factors were calculated using *Tb.Th*, and the influence of the widths of plate-like trabeculae was not considered. Classifying trabeculae into rods or plates may be useful in determining local morphological effects. Furthermore, analyzing the individual thicknesses of trabecula, as Zhao et al. did [9], may improve the prediction accuracy.

This study has several limitations. First, a significant correlation was observed between E_c and *SMI*, suggesting the necessity of investigating the differences in shape factors and elastic moduli between rod- and plate-like trabeculae. Second, the study did not investigate the anisotropy of E_c. Third, in the microcantilever-bending tests, the deflection was applied in a stepwise manner, although the intervals and the number of steps were set to ensure the detection accuracy according to the specimen size. In fact, a sufficiently high linearity was observed. Furthermore, the elastic moduli of the rod-like trabecula specimens were calculated using the formula for a cylinder, which might be a source of error. However, no significant difference was observed between the values obtained in this study and those from previously published microtensile tests, and these variations were also the same [22]. Fourth, the region of interest on which the present measurements were based was a 5-mm cube, and the values obtained might vary depending on the size of the region of interest. Lastly, the cancellous bone and single trabecula specimens were collected from two individuals. Although the animal age and collection sites were the same, the small sample size is a major limitation, and further investigation involving a larger sample size is needed. Furthermore, the effects of aging and disease should also be evaluated in further studies.

5. Conclusions

The present study revealed contributions of the compressive trabecular shape factor and the trabecular orientation and a significant contribution of the bifurcation count to cancellous stiffness, with their combined contributions exhibiting an accuracy as high as that of the bone volume fraction in specific bones with no effects of bone disease or aging. The study identified geometrical features of the microarchitecture that were mechanically important for the cancellous stiffness and indicated their complex contributions underlying bone volume fraction. The findings present experimental insights that could advance the understanding of the mechanism underlying the mechanical function of cancellous bone and provide significant control targets to enhance mechanical functions.

Acknowledgments

This study was supported by JSPS KAKENHI (Grants no. 19K04083, 17K14553, 15H02207, and 22K03803). The authors thank Yuta Kawasaki, Miyu Kobayashi, and Tsugumi Tanaka of Hokkaido University for their technical support.

Competing interests: None declared

Ethical approval: Not required

References

[1] Ulrich D, Van Rietbergen B, Laib A, Rüegsegger P. The ability of three-dimensional structural indices to reflect mechanical aspects of trabecular bone. Bone 1999;25:55–60. https://doi.org/10.1016/s8756-3282(99)00098-8

[2] Greenwood C, Clement JG, Dicken AJ, Evans JPO, Lyburn ID, Martin RM, Rogers KD, Stone N, Adams G, Zioupos P. The micro-architecture of human cancellous bone from fracture neck of femur patients in relation to the structural integrity and fracture toughness of the tissue. Bone Rep 2015;3:67–75. https://doi.org/10.1016/j.bonr.2015.10.001

[3] Bouxsein ML, Boyd SK, Christiansen BA, Guldberg RE, Jepsen KJ, Müller R. Guidelines for assessment of bone microstructure in rodents using micro-computed tomography. J Bone Miner Res 2010;25:1468–86. https://doi.org/10.1002/jbmr.141

[4] Endo K, Yamada S, Todoh M, Takahata M, Iwasaki N, Tadano S. Structural strength of cancellous specimens from bovine femur under cyclic compression. PeerJ 2016;4: e1562. https://doi.org/10.7717/peerj.1562

[5] Liu XS, Sajda P, Saha PK, Wehrli FW, Bevill G, Keaveny TM, Guo XE. Complete volumetric decomposition of individual trabecular plates and rods and its morphological correlations with anisotropic elastic moduli in human trabecular bone. J Bone Miner Res 2008;23:223–35. https://doi.org/10.1359/jbmr.071009

[6] Stauber M, Müller R. Volumetric spatial decomposition of trabecular bone into rods and plates—A new method for local bone morphometry. Bone 2006;38:475–84. https://doi.org/10.1016/j.bone.2005.09.019

[7] Ding M, Lin X, Liu W. Three-dimensional morphometric properties of rod- and plate-like trabeculae in adolescent cancellous bone. J Orthop Translat 2018;12:26–35. https://doi.org/10.1016/j.jot.2017.10.001

[8] Parkinson IH, Badiei A, Stauber M, Codrington J, Müller R, Fazzalari NL. Vertebral body bone strength: the contribution of individual trabecular element morphology. Osteoporos Int 2012;23:1957–65. https://doi.org/10.1007/s00198-011-1832-6

[9] Zhao F, Kirby M, Roy A, Hu Y, Guo XE, Wang X. Commonality in the microarchitecture of trabecular bone: A preliminary study. Bone 2018;111:59–70. https://doi.org/10.1016/j.bone.2018.03.003

[10] Zhou B, Liu XS, Wang J, Lu XL, Fields AJ, Guo XE. Dependence of mechanical properties of trabecular bone on plate–rod microstructure determined by individual trabecula segmentation (ITS). J Biomech 2014;47:702–8. https://doi.org/10.1016/j.jbiomech.2013.11.039

[11] Reznikov N, Chase H, Zvi YB, Tarle V, Singer M, Brumfeld V, Shahar R, Weiner S. Inter-trabecular angle: A parameter of trabecular bone architecture in the human proximal femur that reveals underlying topological motifs. Acta Biomater 2016;44:65–72. https://doi.org/10.1016/j.actbio.2016.08.040

[12] Lucchinetti E, Thomann D, Danuser G. Review Micromechanical testing of bone trabeculae - potentials and limitations. J Mater Sci 2000;35:6057–64. https://doi.org/10.1023/A:1026748913553

[13] Wu D, Isaksson P, Ferguson SJ, Persson C. Young's modulus of trabecular bone at the tissue level: A review. Acta Biomater 2018;78:1–12. https://doi.org/10.1016/j.actbio.2018.08.001

[14] Bini F, Marinozzi A, Marinozzi F, Patanè F. Microtensile measurements of single trabeculae stiffness in human femur. J Biomech 2002;35:1515–9. https://doi.org/10.1016/S0021-9290(02)00182-3

[15] Carretta R, Luisier B, Bernoulli D, Stüssi E, Müller R, Lorenzetti S. Novel method to analyze post-yield mechanical properties at trabecular bone tissue level. J Mech Behav Biomed Mater 2013;20:6–18. https://doi.org/10.1016/j.jmbbm.2012.12.003

[16] Carretta R, Stüssi E, Müller R, Lorenzetti S. Within subject heterogeneity in tissue-level post-yield mechanical and material properties in human trabecular bone. J Mech Behav Biomed Mater 2013;24:64–73. https://doi.org/10.1016/j.jmbbm.2013.04.014

[17] Frank M, Marx D, Nedelkovski V, Fischer JT, Pahr DH, Thurner PJ. Dehydration of individual bovine trabeculae causes transition from ductile to quasi-brittle failure mode. J Mech Behav Biomed Mater 2018;87:296–305. https://doi.org/10.1016/j.jmbbm.2018.07.039

[18] Hernandez CJ, Tang SY, Baumbach BM, Hwu PB, Sakkee AN, Van der Ham F, DeGroot J, Bank RA, Keaveny TM. Trabecular microfracture and the influence of pyridinium and non-enzymatic glycation-mediated collagen cross-links. Bone 2005;37:825–32. https://doi.org/10.1016/j.bone.2005.07.019

[19] McNamara LM, Ederveen AGH, Lyons CG, Price C, Schaffler MB, Weinans H, Prendergast PJ. Strength of cancellous bone trabecular tissue from normal, ovariectomized and drug-treated rats over the course of ageing. Bone 2006;39:392–400. https://doi.org/10.1016/j.bone.2006.02.070

[20] Reisinger AG, Frank M, Thurner PJ, Pahr DH. A two-layer elasto-visco-plastic rheological model for the material parameter identification of bone tissue. Biomech Model Mechanobiol 2020;19:2149–62. https://doi.org/10.1007/s10237-020-01329-0

[21] Rho JY, Ashman RB, Turner CH. Young's modulus of trabecular and cortical bone

material: ultrasonic and microtensile measurements. J Biomech 1993;26:111–9. https://doi.org/10.1016/0021-9290(93)90042-D

[22] Yamada S, Tadano S, Fukuda S. Nanostructure and elastic modulus of single trabecula in bovine cancellous bone. J Biomech 2014;47:3482–7. https://doi.org/10.1016/j.jbiomech.2014.09.009

[23] Busse B, Hahn M, Soltau M, Zustin J, Püschel K, Duda GN, Amling M. Increased calcium content and inhomogeneity of mineralization render bone toughness in osteoporosis: Mineralization, morphology and biomechanics of human single trabeculae. Bone 2009;45:1034–43. https://doi.org/10.1016/j.bone.2009.08.002

[24] Jungmann R, Szabo ME, Schitter G, Tang RY, Vashishth D, Hansma PK, Thurner PJ. Local strain and damage mapping in single trabeculae during three-point bending tests. J Mech Behav Biomed Mater 2011;4:523–34. https://doi.org/10.1016/j.jmbbm.2010.12.009

[25] Ridha H, Thurner PJ. Finite element prediction with experimental validation of damage distribution in single trabeculae during three-point bending tests. J Mech Behav Biomed Mater 2013;27:94–106. https://doi.org/10.1016/j.jmbbm.2013.07.005

[26] Szabó ME, Taylor M, Thurner PJ. Mechanical properties of single bovine trabeculae are unaffected by strain rate. J Biomech 2011;44:962–7. https://doi.org/10.1016/j.jbiomech.2010.12.008

[27] Yamada S, Tadano S, Fukasawa K. Micro-cantilever bending for elastic modulus measurements of a single trabecula in cancellous bone. J Biomech 2016;49:4124–7. https://doi.org/10.1016/j.jbiomech.2016.10.016

[28] Ridler TW, Calvard S. Picture thresholding using an iterative selection method. IEEE Trans Syst Man Cybern 1978;8:630–2. https://doi.org/10.1109/TSMC.1978.4310039

[29] Zhang Y, He Z, Fan S, He K, Li C. Automatic thresholding of micro-CT trabecular bone images. 2008 International Conference on BioMedical Engineering and Informatics 2008;23–7. https://doi.org/10.1109/BMEI.2008.13

[30] Doube M, Kłosowski MM, Arganda-Carreras I, Cordelières FP, Dougherty RP, Jackson JS, Schmid B, Hutchinson JR, Shefelbine SJ. BoneJ: Free and extensible bone image analysis in ImageJ. Bone 2010;47:1076–9. https://doi.org/10.1016/j.bone.2010.08.023

[31] Arganda-Carreras I, Fernández-González R, Muñoz-Barrutia A, Ortiz-De-Solorzano C. 3D reconstruction of histological sections: Application to mammary gland tissue. Microsc Res Tech 2010;73:1019–29. https://doi.org/10.1002/jemt.20829

[32] Lee TC, Kashyap RL, Chu CN. Building skeleton models via 3-D medial surface axis thinning algorithms. CVGIP Graph Models Image Process 1994;56:462–78. https://doi.org/10.1006/cgip.1994.1042

[33] Lekhnitskii SG. Theory of elasticity of an anisotropic elastic body. San Francisco: Holden-Day, Inc.; 1963.

[34] Brear K, Currey JD, Raines S, Smith KJ. Density and temperature effects on some mechanical properties of cancellous bone. Eng Med 1988;17:163–7. https://doi.org/10.1243/EMED_JOUR_1988_017_043_02

[35] Cowper GR. The shear coefficient in Timoshenko's beam theory. J Appl Mech 1966;33:335–40. https://doi.org/10.1115/1.3625046

[36] Prot M, Saletti D, Pattofatto S, Bousson V, Laporte S. Links between mechanical behavior of cancellous bone and its microstructural properties under dynamic loading. J Biomech 2015;48:498–503. https://doi.org/10.1016/j.jbiomech.2014.12.002

Highlights

- Elucidates geometrical features of microarchitecture in cancellous bone mechanics
- Compression testing for 5-mm cubes of bovine femoral cancellous bone
- Combinations of geometrical features accurately expressed cancellous stiffness
- Significant contribution of bifurcation characteristics to cancellous stiffness
- Contributions of trabecular shape and orientation to cancellous stiffness

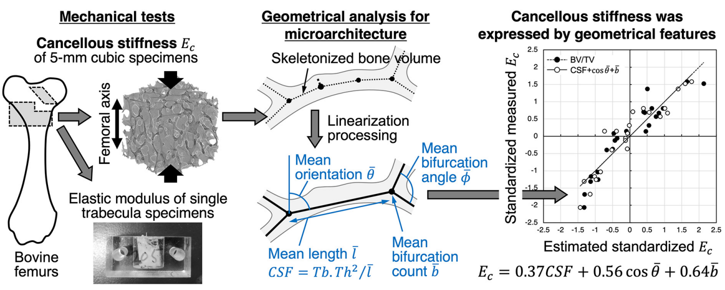
Mechanical tests
Cancellous stiffness E_c
of 5-mm cubic specimens
Femoral axis
Elastic modulus of single
trabecula specimens
Bovine
femurs
Geometrical analysis for
microarchitecture
Skeletonized bone volume
Linearization
processing
Mean
orientation $\bar{\theta}$
Mean
bifurcation
angle $\bar{\phi}$
Mean length $\bar{l}$
$CSF = Tb.Th^2/\bar{l}$
Mean
bifurcation
count $\bar{b}$
Cancellous stiffness was
expressed by geometrical features
BV/TV
CSF+cos $\bar{\theta}$+$\bar{b}$
Standardized measured E_c
Estimated standardized E_c
$E_c = 0.37CSF + 0.56\cos\bar{\theta} + 0.64\bar{b}$

Figure and table legends

Figure 1. (a) Cancellous bone and single trabecula specimens were collected from the shaded regions at the proximal metaphysis and neck of right bovine femurs (Bovines A and B) did not vary significantly in femoral length. (b) Cubic cancellous bone specimens 5 × 5 × 5 mm^3 in size were isolated from Bovine A cut out at the regions vertical to the proximodistal direction of the femur, defined as the femoral axis. The three axes of the cube were aligned to the lateromedial, anteroposterior, and proximodistal directions. (c) Rod-like single trabeculae were isolated from cancellous bone in Bovine B with a portion remaining connected to the other trabeculae. (d) The attached portion of cancellous bone was shaped into a small rectangle. (e) The specimens were placed vertically into a holder and fixed by embedding the cancellous bone portion in epoxy resin.

Figure 2. Schematic diagram of the analysis of cancellous bone microarchitecture. (a) The cubic specimen volume was extracted from micro-CT images and was binarized using ImageJ and BoneJ plug-in to obtain the bone volume. (b) The bone volume was

skeletonized (left), and its branches and junctions were obtained by BoneJ plug-in (right). (c) Subsequently, a network of straight skeletons was obtained by linearizing the skeletonized cancellous bone with artifacts removed using a customized program.

Figure 3. Linearization process of the skeletonized cancellous bone. (a) After removing dots and branches without connections to other branches, short needle-like branches were removed, and bent branches were converted to a straight skeleton. Both ends of the straight skeletons were defined as bifurcation points. (b) In overlapping straight skeletons, one was retained and the others were removed. (c) After removing straight skeletons without connections to other branches, short branches that connected to the junctions connecting three or more branches were removed sequentially, starting from the shortest branch. The branches connected at both ends of the removed short branches were reconnected at the midpoint of the removed branches, which resulted in a new bifurcation point. (d) However, the short branches that were part of a generated triangle were retained to maintain the network structure.

Figure 4. Schematic of a micro-cantilever bending setup. A testing device is customized with a load cell, a uniaxial automatic stage, and a microscope. A loading plate with a taper bore is connected to the load cell. The edge of the bore is contacted to the position adjacent to the free end of a single trabecula specimen. The plate and load cell can be horizontally displaced by the stage as an actuator. Images of the specimen in a vertical position is captured using the microscope for the deflection measurements.

Figure 5. Correlations between E_c and each indicator: (a) *BV/TV*, (b) *CSF*, (c) *BSF*, (d) $\cos\bar{\theta}$, (e) $\bar{b}$, and (f) $\bar{\phi}$. Solid lines indicate regression lines of these relationships.

Figure 6. Correlations between the standardized measured and estimated values of E_c using the regression equations with *BV/TV* or a combination of *CSF*, $\cos\bar{\theta}$, and $\bar{b}$. Black circles and a dashed line indicate the *BV/TV* values and the regression line. White circles and a solid line indicate the values for the combinations and the regression line.

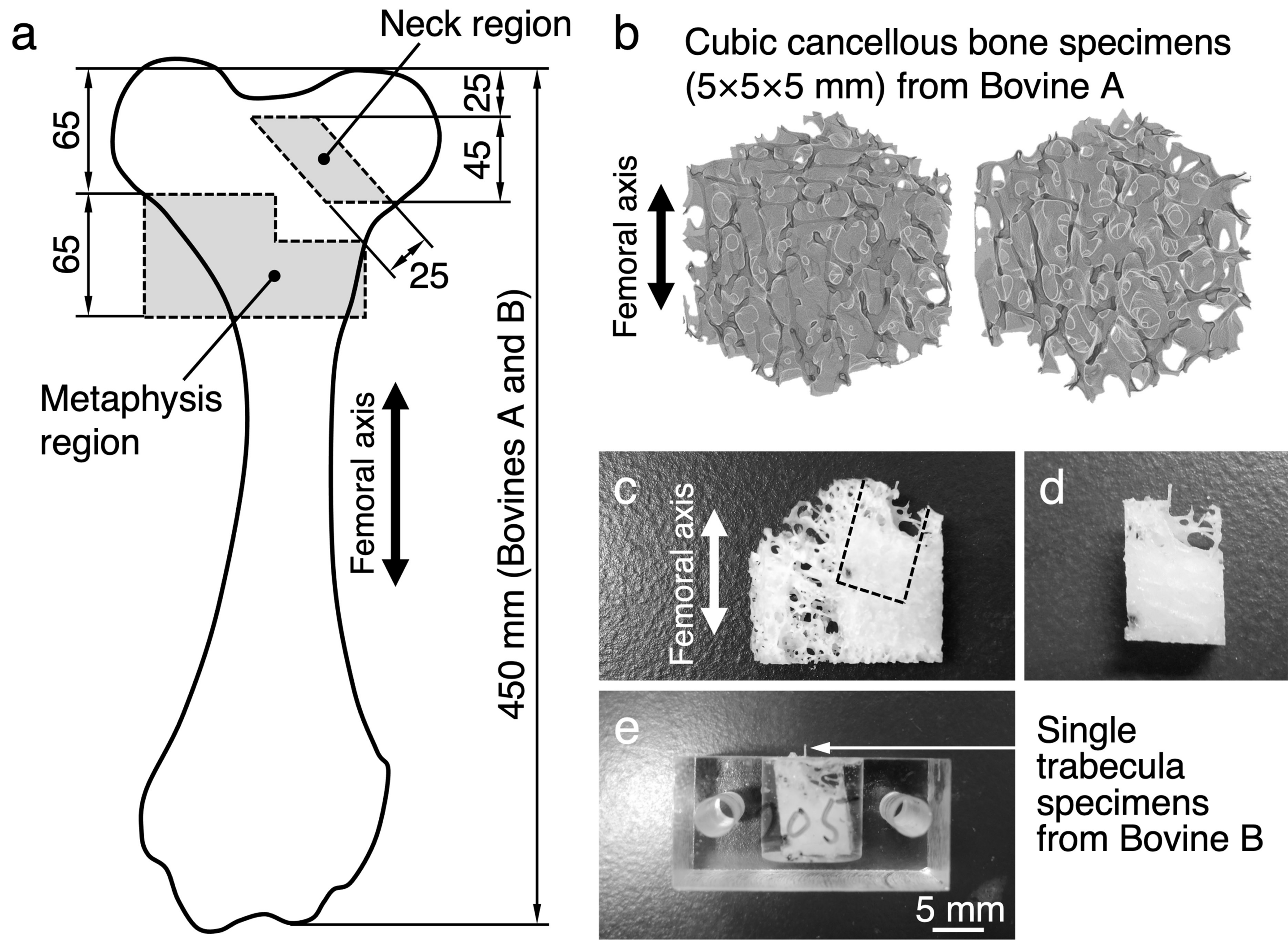
a
Neck region
65
25
45
65
25
Metaphysis region
Femoral axis
450 mm (Bovines A and B)
b
Cubic cancellous bone specimens (5×5×5 mm) from Bovine A
Femoral axis
c
Femoral axis
d
e
Single trabecula specimens from Bovine B
5 mm

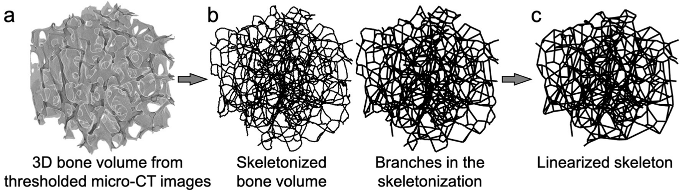
a
b
c
3D bone volume from thresholded micro-CT images
Skeletonized bone volume
Branches in the skeletonization
Linearized skeleton

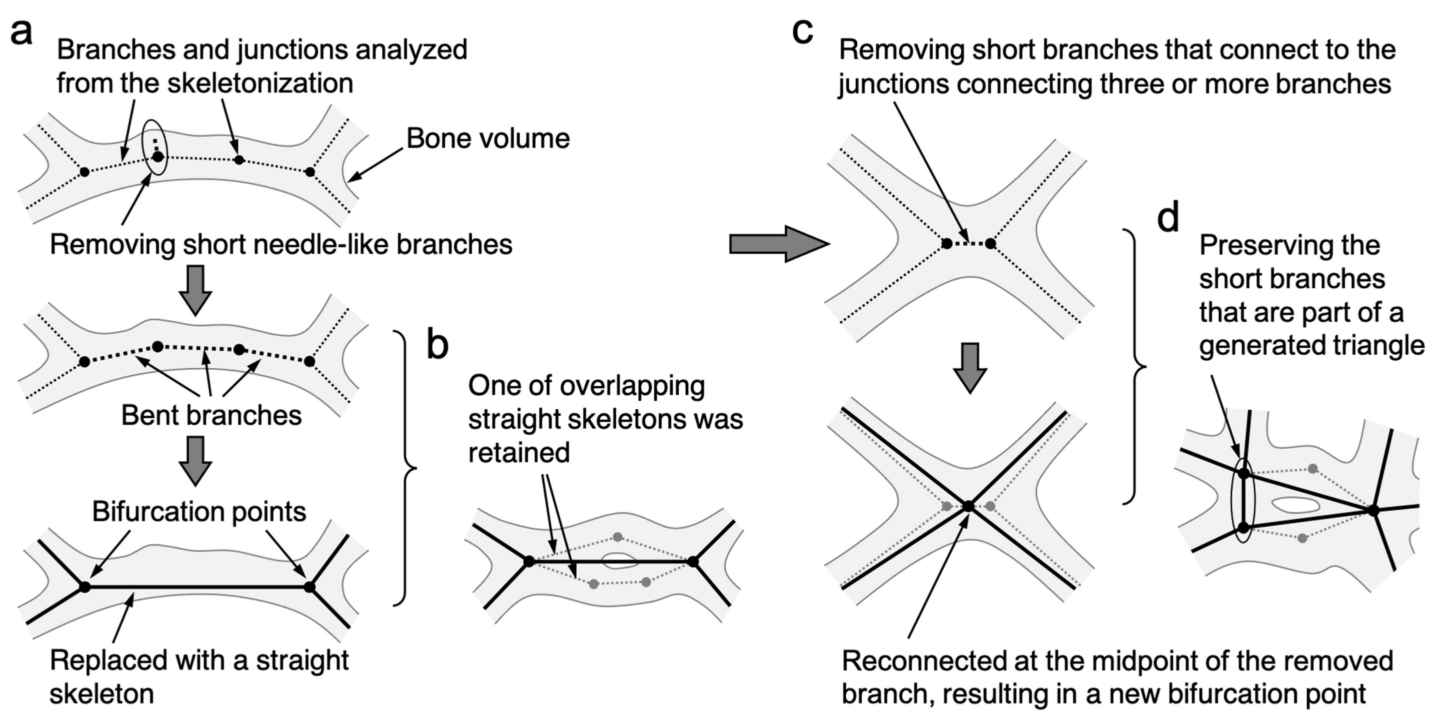
a
Branches and junctions analyzed from the skeletonization
Bone volume
Removing short needle-like branches
Bent branches
Bifurcation points
Replaced with a straight skeleton
b
One of overlapping straight skeletons was retained
c
Removing short branches that connect to the junctions connecting three or more branches
Reconnected at the midpoint of the removed branch, resulting in a new bifurcation point
d
Preserving the short branches that are part of a generated triangle

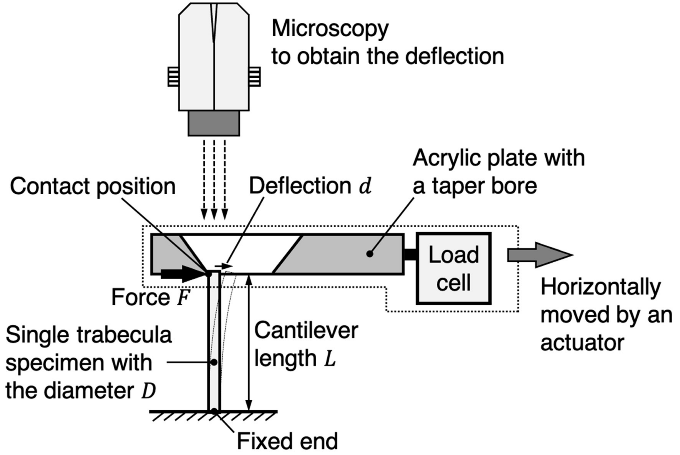

Microscopy
to obtain the deflection
Acrylic plate with
a taper bore
Contact position
Deflection d
Load
cell
Force F
Horizontally
moved by an
actuator
Single trabecula
specimen with
the diameter D
Cantilever
length L
Fixed end

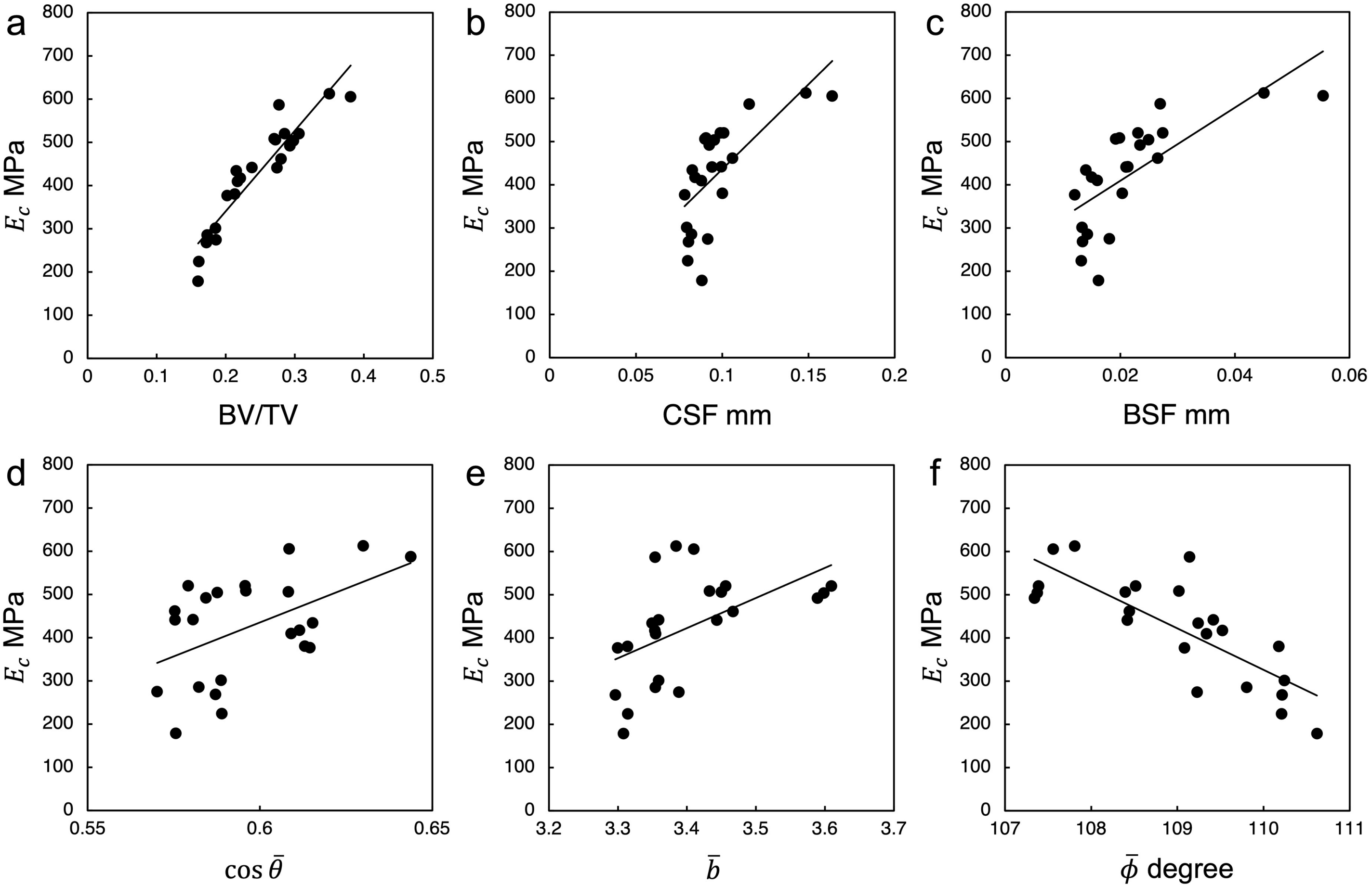
a
b
c
d
e
f
E_c MPa
BV/TV
CSF mm
BSF mm
$\cos\bar{\theta}$
$\bar{b}$
$\bar{\phi}$ degree
0
100
200
300
400
500
600
700
800
0.1
0.2
0.3
0.4
0.5
0.05
0.15
0.02
0.04
0.06
0.55
0.6
0.65
3.2
3.3
3.4
3.5
3.6
3.7
107
108
109
110
111

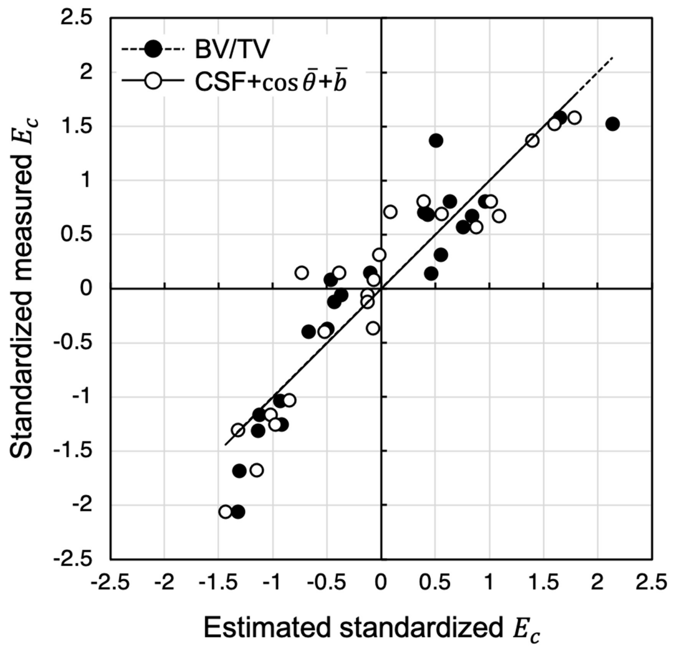
BV/TV
CSF+cos $\bar{\theta}$+$\bar{b}$
Standardized measured E_c
Estimated standardized E_c
2.5
2
1.5
1
0.5
0
-0.5
-1
-1.5
-2
-2.5
-2.5
-2
-1.5
-1
-0.5
0
0.5
1
1.5
2
2.5